IOPscience iopscience.iop.org

Home Search Collections Journals About Contact us My IOPscience

The effect of a Pt impurity layer on the magnetocrystalline anisotropy of hexagonal close-packed Co: a first-principles study

This article has been downloaded from IOPscience. Please scroll down to see the full text article.

2012 J. Phys.: Condens. Matter 24 406001

(http://iopscience.iop.org/0953-8984/24/40/406001)

View the table of contents for this issue, or go to the journal homepage for more

Download details:
IP Address: 152.66.102.74
The article was downloaded on 06/09/2012 at 06:18

Please note that terms and conditions apply.

IOP PUBLISHING JOURNAL OF PHYSICS: CONDENSED MATTER

J. Phys.: Condens. Matter **24** (2012) 406001 (8pp) doi:10.1088/0953-8984/24/40/406001

The effect of a Pt impurity layer on the magnetocrystalline anisotropy of hexagonal close-packed Co: a first-principles study

C J Aas[1], K Palotás[2], L Szunyogh[2,3] and R W Chantrell[1]

[1] Department of Physics, University of York, York YO10 5DD, UK
[2] Department of Theoretical Physics, Budapest University of Technology and Economics, Budafoki út 8., H-1111 Budapest, Hungary
[3] Condensed Matter Research Group of Hungarian Academy of Sciences, Budapest University of Technology and Economics, Budafoki út 8., H-1111 Budapest, Hungary

E-mail: cja505@york.ac.uk

Received 26 June 2012, in final form 15 August 2012
Published 4 September 2012
Online at stacks.iop.org/JPhysCM/24/406001

Abstract

On the basis of the fully relativistic screened Korringa–Kohn–Rostoker method we investigate the variation in the magnetocrystalline anisotropy energy (MAE) of hexagonal close-packed cobalt with the addition of platinum impurities. In particular, we perform calculations on a bulk cobalt system in which one of the atomic layers contains a fractional, substitutional platinum impurity. Our calculations show that at small concentrations of platinum the MAE is reduced, while at larger concentrations the MAE is enhanced. This change in the MAE can be attributed to an interplay between on-site Pt MAE contributions and induced MAE contributions on the Co sites. The latter are subject to pronounced, long-ranged Friedel oscillations that can lead to significant size effects in the experimental determination of the MAE of nanosized samples.

(Some figures may appear in colour only in the online journal)

1. Introduction

Cobalt alloys, such as CoPt or CoPd, are ubiquitous in the field of magnetic recording and of particular interest to the field of ultrafast magneto-optics [1]. In terms of magnetic recording, increasing areal densities require decreased grain size, which in turn requires increasing values of magnetocrystalline anisotropy energy (MAE) to ensure thermal stability of written information [2]. Currently this is achieved using CoPt alloys with perpendicular anisotropy. Consequently an understanding of the origin of the MAE in CoPt is an important practical problem. Since the magnetic properties of these alloys are highly sensitive to the amount and the spatial distribution of the Pt content, understanding the effects of alloying is an important issue. The effects on the magnetic properties of CoPt as functions of the platinum content have been studied extensively, both theoretically [3] and experimentally [4, 5]. Moreover, in recent experimental work [6] it was demonstrated that the MAE of cobalt can be tuned by letting platinum impurities migrate into the cobalt system. Generally it is agreed that the addition of platinum to a magnetic material, such as Fe or Co, influences the magnetic properties, in particular, the MAE of the material primarily through the strong spin–orbit coupling of Pt [7].

The aim of the present work is to elucidate from first principles the effect on the MAE of bulk hcp Co by the addition of platinum. To this end, we use the fully relativistic screened Korringa–Kohn–Rostoker (SKKR) method as combined with the coherent potential approximation (CPA), which is well suited to describing substitutional alloys [8]. Our model focuses on Pt alloying in a (0001) atomic plane of a hcp Co bulk system, from the case of an impurity

© 2012 IOP Publishing Ltd Printed in the UK & the USA

to the case of a complete filling of the layer by Pt. After briefly discussing the computational methods we present the calculated MAE as a function of the Pt concentration and analyze the results in terms of layer- and species-resolved contributions to the MAE. We note that recording media are complex alloy systems, often containing Cr to promote grain boundary separation. It is often found that the maximum MAE as a function of Pt concentration is limited by, for example, the formation of new phases [9] or the presence of stacking faults [10–12]. Here we are concerned only with the intrinsic enhancement of the MAE introduced by the Pt impurities. Remarkably, this analysis highlights the role of long-ranged Friedel oscillations in forming the MAE of the system. Specifically, we demonstrate a layer dependence of the valence charge which makes the effect of the Pt impurities long-ranged. This might have significant impact on the determination of the MAE of thin film samples corresponding to the systems studied in this work. In particular it might be expected to give rise to finite-size effects in the MAE of granular thin films for magnetic recording which would become more significant as the grain size is reduced.

2. Computational details

The central feature of the SKKR method is the evaluation of the electronic Green's function of a layered system. Here, a layered system refers to a system exhibiting two-dimensional translational symmetry in each (infinite) atomic plane, but in which there are no symmetry requirements along the third axis. From the Green's function one can then determine a number of physical quantities of interest, such as site-projected charges, spin and orbital moments and the total energy of the system. As the method is well documented elsewhere [13, 14], here we present only some details of our calculations. The calculations were performed within the local spin-density approximation (LSDA) of density-functional theory (DFT) as parametrized by Vosko *et al* [15] The effective potentials and fields were treated in the framework of the atomic sphere approximation (ASA). The substitutional Pt alloying was treated within the coherent potential approximation (CPA) [8, 16].

The above LSDA–ASA method fails in predicting the orbital moment and the MAE for hcp Co correctly, see also [17]. Although there is an implication that a full-potential treatment improves the agreement with experiment [18], we employed a rather simple, heuristic extension of the relativistic electron theory by the orbital polarization (OP) correction [19–21], as implemented within the KKR method by Ebert and Battocletti [22]. The corresponding Kohn–Sham–Dirac equations were solved using a spherical wave expansion up to an angular momentum number of $\ell = 3$, although the OP correction was applied only for the $\ell = 2$ orbitals. It should be mentioned that orbital polarization effects are more realistically described in terms of the LSDA + U method [23], in particular, using a corrected random-phase approximation treatment for the screened Coulomb interaction [24].

The magnetocrystalline anisotropy energy was evaluated within the magnetic force theorem [17, 25], in which the total energy of the system can be replaced by the single-particle (band) energy. As noted by Nonas *et al* [26] this approach cannot be used if the size of the spin magnetic moments strongly depend on their orientation, as in, for example, the case of magnetic 5d impurities deposited on Ag(001) surface. Moreover, we employed the torque method [27], making use of the fact that, for a uniaxial system, the MAE, K, can be calculated up to second order in spin–orbit coupling as

$$K = E(\theta = 90^\circ) - E(\theta = 0^\circ) = \left.\frac{\mathrm{d}E}{\mathrm{d}\theta}\right|_{\theta=45^\circ}, \qquad (1)$$

where, in the case of hcp geometry, θ denotes the angle of the spin polarization with respect to the (0001) direction, i.e., the direction perpendicular to the hexagonal planes. Note that the $\hat{\mathbf{z}}$-axis of the (global) frame of reference in our calculations is defined to be parallel to the (0001) direction. Within the KKR formalism, K can be decomposed into site- and species-resolved contributions,

$$K = \sum_{i,\alpha} s_i^\alpha D_i^{(\alpha)}, \qquad (2)$$

where s_i^α denotes the concentration of species α at site i and $D_i^{(\alpha)}$ denotes the corresponding derivative of the band energy. Using Lloyd's formula [28], $D_i^{(\alpha)}$ can be calculated as [29]

$$D_i^{(\alpha)} = -\frac{1}{\pi}\,\mathrm{Im}\int^{\epsilon_{\mathrm{F}}^{(\hat{n})}} \mathrm{d}\epsilon\,\mathrm{Tr}\left(\frac{\partial \underline{t}_i^{(\alpha,\hat{\mathbf{n}})}(\epsilon)^{-1}}{\partial\theta}\underline{\tau}_{ii}^{(\alpha,\hat{\mathbf{n}})}(\epsilon)\right), \qquad (3)$$

where $\epsilon_{\mathrm{F}}^{(\hat{n})}$ is the Fermi energy and, in case species α occupies site i, $\underline{t}_i^{(\alpha,\hat{\mathbf{n}})}(\epsilon)$ and $\underline{\tau}_{ii}^{(\alpha,\hat{\mathbf{n}})}(\epsilon)$ stand for the angular momentum matrices of the single-site t operator and the site-diagonal scattering path operator, respectively. All these quantities are calculated at the direction of the magnetization $\hat{\mathbf{n}} = (\frac{1}{\sqrt{2}}, 0, \frac{1}{\sqrt{2}})$, corresponding to $\theta = 45^\circ$ in equation (1). The derivative of the t-matrix is evaluated as described in [30]. The energy integral in equation (3) can be accurately performed by sampling 20 energy points on an asymmetric mesh along a semi-circle contour in the upper complex semi-plane. In order to achieve an accuracy within 5% for the MAE, a sufficiently dense mesh in the two-dimensional Brillouin zone (2D-BZ) was used to evaluate $\underline{\tau}_{ii}^{(\alpha,\hat{\mathbf{n}})}(\epsilon)$: at the energy point closest to the Fermi energy, we used 5764 k-points in the irreducible wedge of the 2D-BZ, corresponding to more than 34 000 k-points in the full 2D-BZ. Due to the two-dimensional translational symmetry of the system, the MAE should be related to a 2D unit cell, therefore, in the following the index i in equation (2) is used to label atomic layers.

The SKKR method as applied to layered systems requires the system to be divided into a middle region wedged between two semi-infinite bulk regions. Adhering to this requirement, the effect of platinum alloying in a single atomic layer of bulk hcp Co was investigated by considering a layered system as shown in figure 1. Each atomic layer in the semi-infinite bulk regions corresponds to pure hcp Co bulk. Since the middle region needs to contain an integer number of unit cells

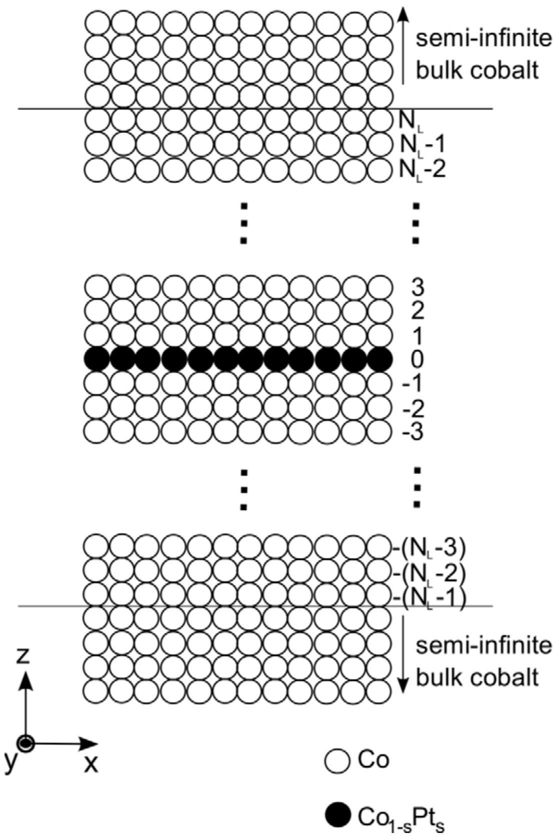

Figure 1. Sketch of the geometry of the system containing N_{L} hcp unit cells, i.e., $2N_{\mathrm{L}}$ atomic layers wedged between two perfect semi-infinite bulk Co systems. In the zero-indexed layer (black circles) a random substitutional alloy with platinum, $\mathrm{Co}_{1-s}\mathrm{Pt}_s$, is considered. Note that the $\hat{\mathbf{z}}$-axis is defined to be parallel to the (0001) direction of the hcp crystal.

and since each unit cell spans two atomic layers, this region consists of $2N_{\mathrm{L}}$ hexagonal Co layers stacked along the (0001) direction. In one of the two central layers of the middle region, namely, in the one indexed by 0 in figure 1, a fraction s of the Co atoms are replaced by Pt atoms. From here on, this layer will be referred to as the impurity layer. It should also be mentioned that in this work no attempts are made to trace any structural relaxation effects of the hcp Co lattice caused by Pt impurities. To support this approach, we note that in [31] the change in the MAE of an FePt slab due to surface relaxation is reported to be only about 5%.

To take into account relaxation of the effective potentials and fields, we performed self-consistent calculations with $N_{\mathrm{L}} = 14$, i.e. for 28 layers in total. One important consequence of the geometrical construction shown in figure 1 is that the calculation of K in equation (2) is confined to layers within the middle region, i.e., for $-(N_{\mathrm{L}} - 1) \le i \le N_{\mathrm{L}}$. This means that the long-ranged Friedel oscillations that arise due to the presence of Pt impurities are necessarily truncated. In order to safeguard against any numerical artifacts caused by this truncation, we increased the number of atomic layers in the middle region until the layer-resolved MAE converged to within about 1% accuracy to the bulk Co MAE at the outer edges of the middle region. According to our calculations (see below), this condition requires $N_{\mathrm{L}} = 40$, i.e., 80 atomic layers in total. We performed these calculations of the MAE by appending the perfect bulk potential of hcp Co to the layers $-39 \le i \le -14$ and $15 \le i \le 40$, i.e., neglecting self-consistency effects for these atomic layers. To check the accuracy of this approach, we compared $D_i^{(\mathrm{Co})}$ for atomic layer no. 14 (with relaxed self-consistent potential) with that for atomic layer no. -14 (with appended Co bulk potential) and obtained that the two values agree to within 0.02%.

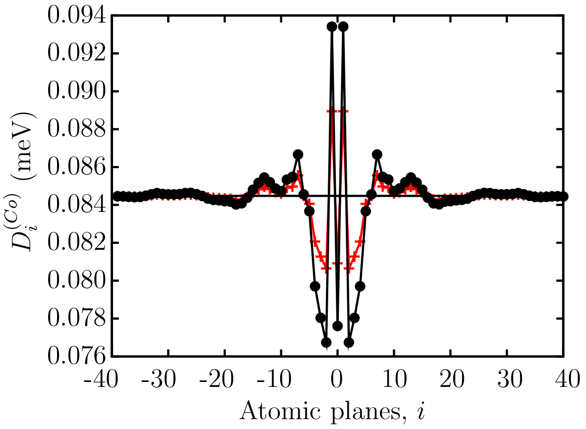

Figure 2. Calculated layer-resolved Co contributions, $D_i^{(\mathrm{Co})}$, to the MAE, see equation (3), across the system shown in figure 1 for $s = 0.01$ (red +) and $s = 0.02$ (black ●). The MAE of bulk Co is indicated by the solid black horizontal line. Solid lines connecting the symbols serve as guides for the eye.

3. Results and discussion

To test our computational method, we first determined the MAE of bulk hcp Co. Excluding the OP correction we obtained an easy-plane magnetization and a MAE of 6.7 μeV/Co atom, while including the OP correction we instead obtained an easy axis perpendicular to the hexagonal Co planes and a MAE of 84.4 μeV/Co. The latter result is in good agreement with the experimental value of 65.5 μeV [32] and with the experimental easy axis being along the (0001) direction. Our result also compares well with that of Trygg *et al* [18], who calculated $K = 110$ μeV for hcp Co using a full-potential LMTO method including OP correction.

As described in section 2, we performed calculations of the MAE of a bulk Co system in which a single layer has been substitutionally alloyed by Pt in a fraction of $0 < s \le 1$. The layer-resolved Co contributions to the MAE, $D_i^{(\mathrm{Co})}$, see equations (2) and (3), are shown in figure 2 for $s = 0.01$ and $s = 0.02$. Remarkably, even such small amounts of Pt induce large fluctuations in $D_i^{(\mathrm{Co})}$: in the impurity layer ($i = 0$) and in the Co layers near the impurity layer ($1 \le |i| \le 4$) the relative changes of $D_i^{(\mathrm{Co})}$ with respect to the bulk Co MAE reach 10%. In particular, the Co contribution from layers $i = \pm 1$ is enhanced to nearly 94 μeV, while that those from layers $i = \pm 2$ are reduced to nearly 76 μeV for $s = 0.02$. For layers further away from the impurity layer ($|i| \ge 5$), oscillations in $D_i^{(\mathrm{Co})}$ with rapidly decreasing amplitude can be seen. Reassuringly, the layer-resolved Co contributions approach the bulk Co MAE towards the outer edges of the

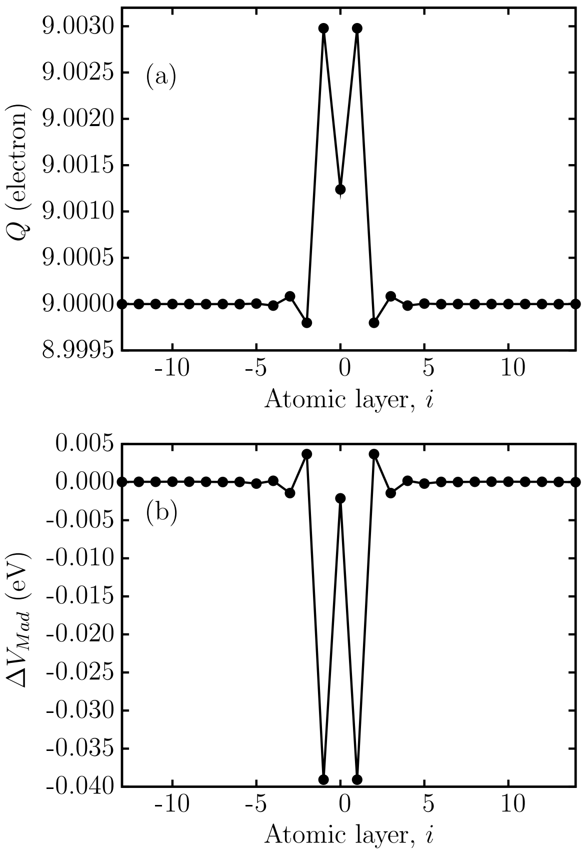

Figure 3. (a) Calculated valence charge on the Co atoms, Q, and (b) relative shift of the Madelung potentials with respect to the bulk case, ΔV_{Mad}, for layers $-13 \le i \le 13$ and for a Pt concentration, $s = 0.02$. Solid lines serve as guides for the eye.

middle region chosen in our calculations ($i \to N_{\mathrm{L}} = 40$ and $i \to -(N_{\mathrm{L}} - 1) = -39$). The mirror symmetry around the impurity layer, $D_i^{(\mathrm{Co})} = D_{-i}^{(\mathrm{Co})}$, is also fulfilled with a high accuracy.

Our earlier studies of the MAE of impurities [33, 34], justified that the MAE is extremely sensitive to the presence of Friedel oscillations in the charge density. It is, therefore, tempting to relate figure 2 to the change in the valence charge on the Co atoms with respect to the distance from the impurity layer. From figure 3(a) we can see that the Co atoms in the impurity layer and, in particular, the Co atoms in layers adjacent the impurity layer gain some extra charge, while the charge transfer to more distant Co layers drops rapidly. The energy shift of the layer-resolved Co valence band position is well described by the layer-resolved change in the Madelung potential. (Note that within the ASA the Madelung potential in each atomic plane is a constant.) As is obvious from figure 3(b), an enhanced (reduced) charge at the Co sites is accompanied with a downward (upward) shift of the valence states. Comparing with figure 2, this shift of the valence states correlates directly with the MAE contributions of the Co layers adjacent the impurity layer, but, clearly enough, the changes in the MAE contributions from more distant Co layers are also subject to fine details of the valence states influenced by the Pt alloying.

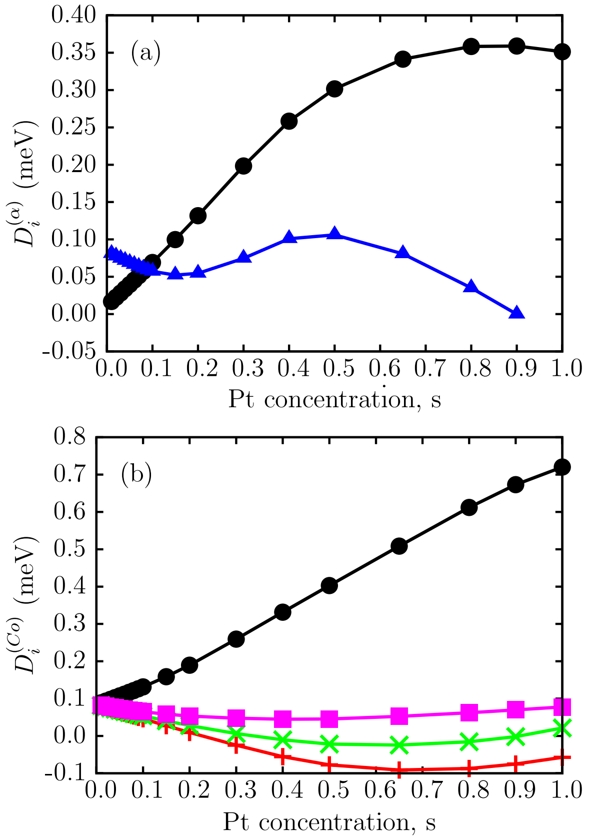

Figure 4. Calculated species-resolved MAE contributions (a) for the impurity layer: $D_0^{(\mathrm{Pt})}$ (black ●) and $D_0^{(\mathrm{Co})}$ (blue ▲) and (b) for Co layers: $D_1^{(\mathrm{Co})}$ (black ●), $D_2^{(\mathrm{Co})}$ (red +), $D_3^{(\mathrm{Co})}$ (green ×) and $D_4^{(\mathrm{Co})}$ (purple ■). Solid lines connecting the symbols serve as guides for the eye.

The effect on the species-resolved MAE by alloying with Pt is demonstrated for the whole range of s in figure 4, showing $D_i^{(\mathrm{Co})}$ for layers $0 \le i \le 4$, together with the direct contribution of Pt, $D_0^{(\mathrm{Pt})}$. In the impurity layer $i = 0$, see figure 4(a), the Co contribution $D_0^{(\mathrm{Co})}$ is reduced by the addition of Pt for concentrations up to about $s = 0.15$ and then enhanced for concentrations $0.15 < s < 0.50$. For concentrations $s > 0.50$, $D_0^{(\mathrm{Co})}$ is again reduced with increasing s and at $s \approx 0.9$, $D_0^{(\mathrm{Co})}$ even becomes negative. Note that $D_0^{(\mathrm{Co})}$ for $s \to 1$ (not calculated here) would correspond to the contribution of a single Co atom in a pure Pt layer which, in general, would differ from zero. The on-site platinum contribution, $D_0^{(\mathrm{Pt})}$, approaches the very small value of 0.01 meV as $s \to 0$, rapidly increases up to 0.30 meV at $s \approx 0.5$ and then saturates at $D_0^{(\mathrm{Pt})} \approx 0.35$ meV for larger s.

It can be inferred from figure 4(b), that Pt alloying most dramatically influences the Co contribution at the layers adjacent to the impurity layer: $D_1^{(\mathrm{Co})}$ increases almost linearly from the bulk MAE at $s = 0$ to about 0.7 meV at $s = 1$. As already seen in figure 2, the Co contributions $D_i^{(\mathrm{Co})}$ from layers further out ($2 \le i \le 4$) decrease with increasing s and even becomes negative at $s \approx 0.25$ for $i = 2$ and 3. For $s > 0.5$

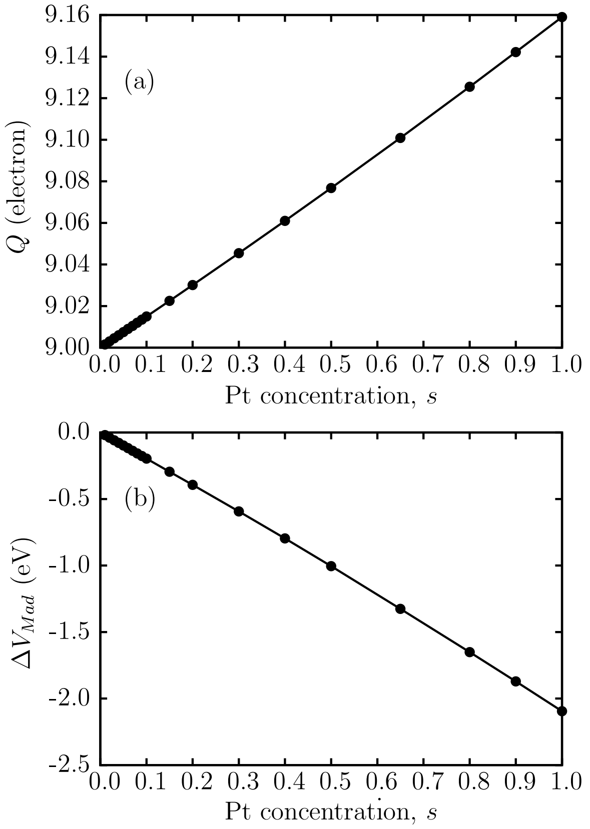

Figure 5. (a) Calculated valence charge on the Co atom, Q, and (b) relative shift of the Madelung potential with respect to the bulk case, ΔV_{Mad}, for layer 1 as a function of the Pt concentration, s. Solid lines serve as guides for the eye.

these contributions show a modest increase, but $D_2^{(\mathrm{Co})}$ still remains negative.

It is worth investigating the change of valence states projected onto the Co atoms in layer 1. From figure 5(a) it is obvious that the valence charge at this Co atom increases almost linearly with s from 9.00 e to 9.16 e. This increase in the valence charge is necessarily accompanied by a downshift of the corresponding valence states, as characterized by the change in the Madelung potential, which is also linear s, see figure 5(b). The large enhancement of the MAE contribution from layer 1, $D_1^{(\mathrm{Co})}$, can therefore be related directly to the monotonic shift of the corresponding valence states.

The dependence of the MAE of hcp Co on the band-filling was investigated in [17] and, in the range of $9 \leq Q \lesssim 9.2$, a much weaker dependence was obtained as for $D_1^{(\mathrm{Co})}$, see figure 4(b). The main difference between the two studies is that in our case the change in the band-filling is accompanied by the breaking of the bulk symmetry upon the addition of Pt atoms, giving rise to an enhanced uniaxial magnetic anisotropy when a complete Pt layer is being formed. A similar argument seems to apply for the rapid increase in the on-site contribution of Pt, see figure 4(a). Furthermore, we stress that our calculations rely on a non-perturbative treatment of spin–orbit coupling, therefore, unlike to [35], it is not obvious to relate a simple microscopic mechanism to the spatial and species-resolved decomposition of the MAE. According to [34] we can, however, suppose that the spin-polarized valence electrons at the Co sites experience strong spin–orbit coupling upon hybridizing with mobile conduction electrons that scatter on Pt sites. This picture is consistent with the large enhancement of $D_1^{(\mathrm{Co})}$ with increasing Pt concentration.

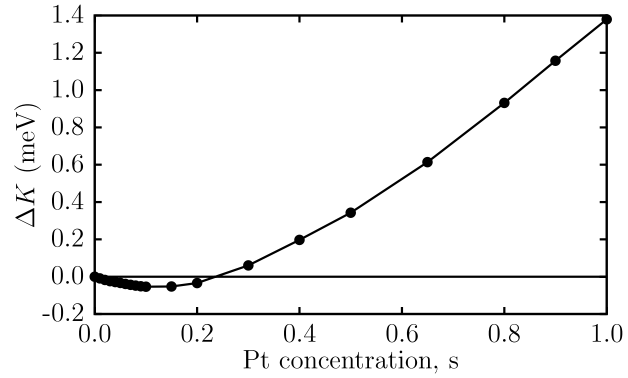

Figure 6. The change in the MAE, ΔK, of a system of 81 atomic layers, see equation (4), as a function of the Pt concentration, s. The solid line connecting the symbols serves as a guide for the eye.

While the species- and layer-resolved contributions to the MAE are very illuminating for a microscopic description of the variations in the MAE, from an experimental point of view only the MAE of the whole system can be accessed. Here, this means considering the MAE of the entire middle region illustrated in figure 1 for $N_{\mathrm{L}} = 40$. In order to extract the change in this MAE induced by the Pt impurities, we define the excess MAE, $\Delta K(s)$, by subtracting the MAE of the 'unperturbed' cobalt bulk layers,

$$\Delta K(s) = sD_0^{(\mathrm{Pt})} + (1-s)D_0^{(\mathrm{Co})} + 2\sum_{i=1}^{40} D_i^{(\mathrm{Co})} - 81K_{\mathrm{Co}}, \tag{4}$$

where K_{Co} is the calculated MAE of hcp bulk Co (84.4 μeV). Note that we have taken into account the off-center positioning of the impurity layer by doubling the Co contributions $D_i^{(\mathrm{Co})}$ for $i \in [1, 40]$, thus, in total, a system of 81 layers is considered.

ΔK is shown as a function of s in figure 6, demonstrating that for small concentrations of platinum ($s < 0.24$) the addition of platinum to bulk cobalt actually reduces the total MAE of the system by about 80 μeV. This is in strong contrast to the on-site contribution of Pt, $D_0^{(\mathrm{Pt})}$, being positive for all values of s as seen in figure 4(a). The reduction in MAE for low s, therefore, stems from the decrease in the cobalt contributions $D_i^{(\mathrm{Co})}$ with increasing s, in particular, for $i = 0, 2, 3$ and 4, see figure 4. ΔK becomes positive for $s > 0.24$ as the increasing on-site contribution, $D_0^{(\mathrm{Pt})}$, gets larger weight (note that it is multiplied by s) and due to the large enhancement of $D_1^{(\mathrm{Co})}$. At $s = 1$, $\Delta K = 1.4$ meV, which is approximately four times the on-site platinum contribution, $D_0^{(\mathrm{Pt})} \approx 0.35$ meV for $s = 1$.

For nanosized systems, it might be of interest to consider the change in the MAE per platinum atom in the system, $\bar{K}_{\mathrm{Pt}}$,

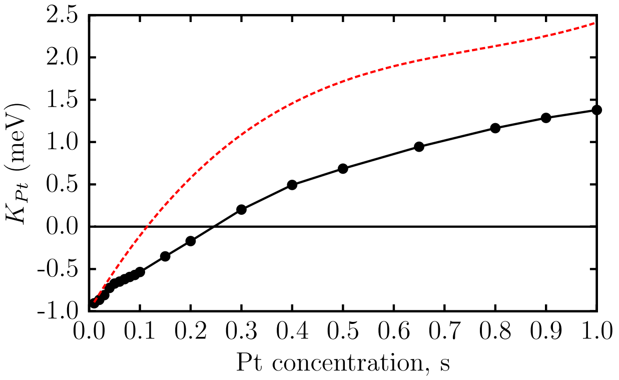

Figure 7. Black circles: calculated change in the MAE per Pt atom, $\bar{K}_{\rm Pt}$, see equation (5), as a function of the Pt concentration, s. The black solid line connecting the symbols serves as a guide for the eye. Red dashed line: the change in the MAE per Pt atom added, $K_{\rm Pt}$, see equation (6), as calculated from a polynomial fit of $\Delta K(s)$ in figure 6.

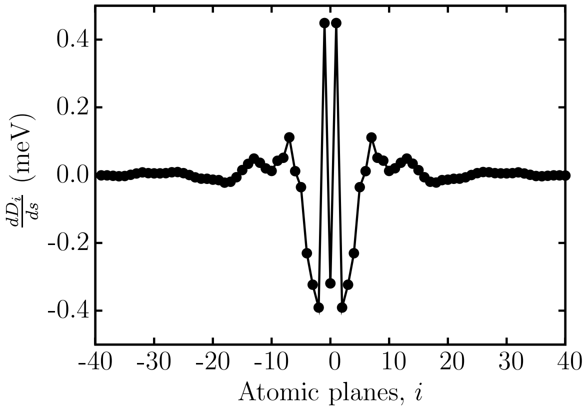

Figure 8. Calculated derivatives of the layer-resolved Co contributions to the MAE, equation (8), for the Pt concentration $s = 0.02$. The solid line serves as a guide for the eye.

defined by

$$\bar{K}_{\rm Pt}(s) = \frac{\Delta K(s)}{s}, \tag{5}$$

and also, the change in the MAE per platinum atom added to the system, $K_{\rm Pt}$, obviously given by

$$K_{\rm Pt}(s) = \frac{{\rm d}(\Delta K(s))}{{\rm d}s}. \tag{6}$$

We obtained $K_{\rm Pt}(s)$ by fitting a fourth-order polynomial to the function $\Delta K(s)$ in figure 6 and then finding the derivative of this function analytically. As apparent from figure 7, both $\bar{K}_{\rm Pt}$ and $K_{\rm Pt}$ are monotonically increasing with increasing s, starting with the same value of about -1 meV at $s = 0$ (see later). It follows directly from figure 6, that $\bar{K}_{\rm Pt}$ crosses zero at $s \approx 0.24$, while $K_{\rm Pt}$ crosses zero at $s \approx 0.11$ (i.e. where the function $\Delta K(s)$ reaches its minimum). For a complete platinum layer immersed in bulk cobalt, i.e. for $s = 1$, $\bar{K}_{\rm Pt} = \Delta K \approx 1.4$ meV. A comparison with figure 4 shows that about 25% of this value arises from the direct contribution of Pt, $D_1^{(\rm Pt)}$, and the rest from the induced contributions at the Co atoms. Interestingly, the change in the MAE by addition of a Pt atom to the system, $K_{\rm Pt}$, exhibits a surprisingly large value of about 2.5 meV at $s = 1$. From figure 4(a) it can be inferred that the on-site Pt contribution $D_0^{(\rm Pt)}$ has nearly zero slope in this region of s, thus, this large value of $K_{\rm Pt}$ stems mainly from an increase in $D_i^{(\rm Co)}$ for $1 \leq |i| \leq 4$ near $s = 1$.

In the limit $s \to 0$, corresponding to the case of a single Pt impurity in bulk Co, $\bar{K}_{\rm Pt}$ and $K_{\rm Pt}$ should be identical, since for small s the function $\Delta K(s)$ exhibits, in principle, a linear dependence. This is fairly well confirmed by our calculations. $K_{\rm Pt}(0)$ can then be expressed as

$$K_{\rm Pt}(0) = D_0^{(\rm Pt)}(0) - K_{\rm Co} + \sum_{i=-40}^{40} \left.\frac{{\rm d}D_i^{(\rm Co)}(s)}{{\rm d}s}\right|_{s=0}. \tag{7}$$

The physical meaning of the above equation is that adding a Pt impurity to bulk Co has two effects on the MAE of the system: the first two terms, $D_0^{(\rm Pt)}(0) - K_{\rm Co}$, represent the direct contribution of a Co atom being replaced by a Pt atom, whereas the last term of equation (7) quantifies the induced change in the MAE contributions from the Co atoms that are not being replaced by Pt. Since the direct contribution is about -0.07 meV, see also figure 4(a), the value of $K_{\rm Pt}(0) = -1$ meV can again only be explained by the induced Co contributions.

In figure 8 we show the approximate layer-resolved derivatives calculated as

$$\left.\frac{{\rm d}D_i^{(\rm Co)}(s)}{{\rm d}s}\right|_{s_j} = \frac{D_i^{(\rm Co)}(s_{j+1}) - D_i^{(\rm Co)}(s_{j-1})}{s_{j+1} - s_{j-1}}, \tag{8}$$

for $s_j = 0.02$ with j indexing the Pt concentrations in ascending order. Clearly, this figure is closely related to figures 2 and 4: for small s, the Co contributions $\{D_i^{(\rm Co)}\}$ show an increasing tendency with increasing s for $|i| = 1$ and $|i| \geq 7$, while they decrease for $2 \leq |i| \leq 5$. Apparently, this latter effect overcomes the former one, leading to the relatively large value of $K_{\rm Pt}(0) = -1$ meV.

We also investigated possible effects of the Friedel oscillations on the MAE by truncating the sum in equation (4) and considering the variation in $\bar{K}_{\rm Pt}$ against the number N of Co planes included in the sum,

$$\bar{K}_{\rm Pt}(s,N) = \frac{1}{s}\Bigg(sD_0^{(\rm Pt)} + (1-s)D_0^{(\rm Co)} + 2\sum_{i=1}^{N} D_i^{(\rm Co)} - (2N+1)K_{\rm Co}\Bigg), \tag{9}$$

for $1 \leq N \leq 40$. The function $\bar{K}_{\rm Pt}(N)$ for $s = 0.01, 0.05, 0.10$ and 0.20 is shown in figure 9. For all cases, the maximum of $\bar{K}_{\rm Pt}(N)$ occurs at $2N + 1 = 3$ planes, i.e. including only one Co layer on each side of the impurity layer. This is because the induced effect on $D_1^{(\rm Co)}$ by the addition of platinum is strongly positive for all s, see figures 2 and 4(b). There is a significant minimum in the calculated $\bar{K}_{\rm Pt}(N)$ at $2N + 1 \approx 11$ planes. Comparing with figure 2, it is obvious that this minimum is due to the reduction of $D_i^{(\rm Co)}$ for $3 \leq |i| \leq 5$ caused by

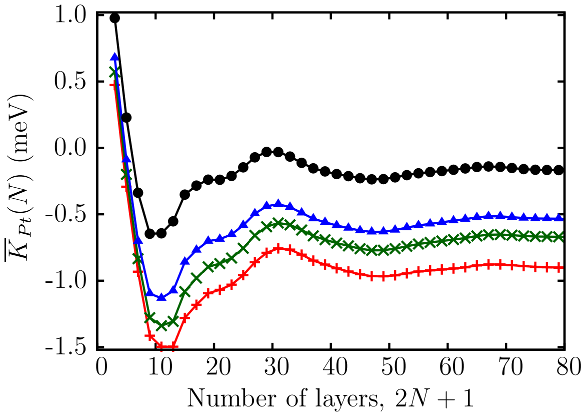

Figure 9. Calculated excess MAE per platinum atom, $\bar{K}_{\mathrm{Pt}}$, as a function of the number of planes N included in the sum in equation (9) for $s = 0.01$ (red +), $s = 0.05$ (green ×), $s = 0.10$ (blue ▲) and $s = 0.20$ (black ●).

the addition of Pt. $\bar{K}_{\mathrm{Pt}}(N)$ then exhibits a local maximum at $2N+1 \approx 31$, mostly due to the Co contributions in layers $8 \leq |i| \leq 15$ counterbalancing the Co contributions of opposite sign in layers $3 \leq |i| \leq 5$. Concerning the overall accuracy of the calculated MAE, the effects of the Friedel oscillations remain significant for about $2N + 1 < 70$ planes, i.e. for 35 layers on either side of the impurity layer. In general, the variation in $\bar{K}_{\mathrm{Pt}}$ with N spans more than 1.5 meV for all values of s. This of course has significant implications for measuring the MAE in thin film samples, as up to about $2N + 1 < 40$ planes, i.e. for film thicknesses $d < 8$ nm, the change in the MAE induced by the Pt impurities located at the center of the sample, is expected to be extremely sensitive on the film thickness. Note that this finite-size effect is superimposed on and, most likely, amplified by quantum interferences arising from the boundaries of the finite film sample [31].

It should be noted that, being a mean-field approach, the CPA completely neglects both structural and electronic short-range-order effects. Such short-range-order effects are likely to be most strongly pronounced for small Pt concentrations s. Therefore, our results in the low-s limit should be tested against another method. By employing a fully relativistic real-space embedded cluster Green's function technique as combined with the SKKR method [36] we made an attempt to test the effect of electronic relaxations around a Pt impurity placed in hcp bulk Co. We performed self-consistent calculations for a cluster containing a Pt impurity and the neighboring Co atoms up to three nearest neighbor (NN) distances of the hcp lattice (a_{NN}). Note that our embedded cluster included 158 Co atoms around the central Pt atom, sorted out geometrically as follows: (i) 36, 2 × 30, 2 × 19 and 2 × 12 Co atoms in layers 0, ±1, ±2 and ±3, and (ii) 12, 56 and 158 Co atoms within the spheres centered around the Pt site having the radii of a_{NN}, $2a_{\mathrm{NN}}$ and $3a_{\mathrm{NN}}$, respectively. The MAE for this cluster was again calculated using the magnetic force theorem. By summing up all the site-resolved contributions of the MAE in the cluster within the spheres as mentioned above, we obtained the values for K_{Pt}, 0.67 meV, -0.31 meV and -0.38 meV, respectively. Obviously, a direct comparison of these values with those for the layered system is hardly possible, since, according to the geometrical classification (i), the K_{Pt} for the cluster refers to an incomplete summation over sites in the respective layers. Nevertheless, comparing with the values in figure 9 related to $2N + 1 = 3, 5$ and 7 and for the concentration of $s = 0.01$ being closest the case of an impurity, we can conclude that both the trend and the magnitude of K_{Pt} are in satisfactory agreement between the CPA and the real-space calculations.

4. Summary and conclusions

Using the fully relativistic screened Korringa–Kohn–Rostoker method combined with the coherent potential approximation, we have studied the MAE of a bulk hcp Co system in which one of the (0001) atomic plane has been alloyed with Pt for the whole concentration range, $0 < s \leq 1$. We conclude that low concentrations of platinum reduce the overall MAE of this system and that the origin of this reduction are the induced changes in the MAE contributions from the Co atoms. In the limit $s \rightarrow 0$ (bulk Co), the change in MAE per platinum atom added is approximately -1 meV. At larger concentrations, the direct MAE contribution of the platinum, which is positive for all Pt concentrations, starts to increase, but the overall change in MAE due to the addition of platinum is still dominated by induced Co contributions. Interestingly, in the limit of a completely filled Pt layer, addition of one Pt atom increases the MAE of the system by about 2.5 meV. We also investigated the effect of long-ranged Friedel oscillations and established a large sensitivity of the MAE on the number of Co layers included in the calculations. This might have a significant impact on the experimental determination of the MAE in thin film samples of this type of system.

Acknowledgments

CJA is grateful to EPSRC and to Seagate Technology for the provision of a research studentship. Support of the EU under FP7 contract NMP3-SL-2012-281043 FEMTOSPIN is gratefully acknowledged. Financial support was in part provided by the New Széchenyi Plan of Hungary Project ID. TÁMOP-4.2.2.B-10/1–2010-0009 and the Hungarian Scientific Research Fund (contracts OTKA PD83353, K77771). KP benefited the Bolyai Research Grant of the Hungarian Academy of Sciences. Support of the HAS Wigner Research Centre of Physics through the usage of its computational facilities is also kindly acknowledged.

References

[1] Lu B, Klemmer T, Wierman K, Ju G P, Weller D, Roy A G, Laughlin D E, Chang C H and Ranjan R 2002 *J. Appl. Phys.* **91** 8025

[2] Weller D, Moser A, Folks L, Best M E, Lee W, Toney M F, Schwickert M, Thiele J-U and Doerner M F 1999 *IEEE Trans. Magn.* **36** 10

[3] Razee S S A, Staunton J B and Pinski F J 1997 *Phys. Rev.* B **56** 8082

[4] Aboaf J A, Herd S R and Klokholm E 1983 *IEEE Trans. Magn.* **4** 1514

[5] Miller M S, Schultz A E, Chow Y M and Heuer L A 1994 *Surf. Coat. Technol.* **68/69** 696

[6] Jaworowicz J *et al* 2009 *Appl. Phys. Lett.* **95** 022502

[7] Abes M, Venuat J, Carvalho A, Arabski J, Muller D, Schmerber G, Beaurepaire E, Panissod P, Dinia A and Pierron-Bohnes V 2005 *J. Magn. Magn. Mater.* **286** 297

[8] Gyorffy B 1972 *Phys. Rev.* B **5** 2382

[9] Toney M F, Marinero E E, Doerner M F and Rice P M 2003 *J. Appl. Phys.* **94** 4018

[10] Ishikawa A and Sinclair R 1996 *IEEE Trans. Magn.* **32** 3605

[11] Ishikawa A and Sinclair R 1996 *J. Magn. Magn. Mater.* **152** 265

[12] Sokalski V, Laughlin D E and Zhu J-G 2011 *J. Appl. Phys.* **110** 093919

[13] Zabloudil J, Hammerling R, Szunyogh L and Weinberger P 2005 *Electron Scattering in Solid Matter* (Berlin: Springer)

[14] Ebert H, Ködderitzsch D and Minár J 2011 *Rep. Prog. Phys.* **74** 096501

[15] Vosko S H, Wilk L and Nusair M 1980 *Can. J. Phys.* **58** 1200

[16] Soven P 1967 *Phys. Rev.* **156** 809

[17] Daalderop G H O, Kelly P J and Schuurman M 1991 *Phys. Rev.* B **44** 12054

[18] Trygg J, Johansson B, Eriksson O and Wills J M 1995 *Phys. Rev. Lett.* **75** 2871

[19] Brooks M S S 1985 *Physica* B **130** 6
Eriksson O, Johansson B and Brooks M S S 1989 *J. Phys.: Condens. Matter* **1** 4005
Eriksson O, Brooks M S S and Johansson B 1990 *Phys. Rev.* B **41** 7311

[20] Eschrig H 1996 *The Fundamentals of Density Functional Theory* (Leipzig: Teubner)

[21] Eschrig H, Sargolzaei M, Koepernik K and Richter M 2005 *Europhys. Lett.* **72** 611

[22] Ebert H and Battocletti M 1996 *Solid State Commun.* **98** 785

[23] Solovyev I V, Liechtenstein A I and Terakura K 1998 *Phys. Rev. Lett.* **80** 5758

[24] Solovyev I V 2005 *Phys. Rev. Lett.* **95** 267205

[25] Jansen H J F 1999 *Phys. Rev.* B **59** 4699

[26] Nonas B, Cabria I, Zeller R, Dederichs P H, Huhne T and Ebert H 2001 *Phys. Rev. Lett.* **86** 2146

[27] Wang X, Wu R, Wang D and Freeman A J 1996 *Phys. Rev.* B **54** 61

[28] Lloyd P 1967 *Proc. Phys. Soc.* **90** 207

[29] Staunton J B, Szunyogh L, Buruzs A, Gyorffy B L, Ostanin S and Udvardi L 2006 *Phys. Rev.* B **74** 144411

[30] Udvardi L, Szunyogh L, Palotás K and Weinberger P 2003 *Phys. Rev.* B **68** 104436

[31] Zhang H, Richter M, Koepernik K, Opahle I, Tasnádi F and Eschrig H 2009 *New J. Phys.* **11** 043007

[32] Stearns M B 1986 *3D, 4D, and 5D Elements, Alloys and Compounds* (Berlin: Springer)

[33] Szunyogh L and Gyorffy B L 1997 *Phys. Rev. Lett.* **78** 3765–8

[34] Szilva A, Gallego S, Munoz M C, Gyorffy B L, Zarand G and Szunyogh L 2008 *Phys. Rev.* B **78** 195418

[35] Solovyev I V, Dederichs P H and Mertig I 1995 *Phys. Rev.* B **52** 13419

[36] Lazarovits B, Szunyogh L and Weinberger P 2002 *Phys. Rev.* B **65** 104441